A Flexible Low Power Subsampling UWB Receiver Based on Line Spectrum Estimation Methods

Yves Vanderperren, Wim Dehaene
Katholieke Universiteit Leuven, Belgium
EE Dept. (ESAT-MICAS)
Email: {yves.vanderperren,wim.dehaene}@esat.kuleuven.be

Geert Leus
Delft University of Technology, The Netherlands
Faculty of EE, Mathematics and Computer Science
Email: leus@cas.et.tudelft.nl

***Abstract*— This paper presents a low power pulsed UWB receiver sampling below Nyquist rate which can accomodate time-varying data rate and quality-of-service requirements for applications communicating via UWB. The performance of pulse amplitude and pulse position modulations is assessed in AWGN and dense multipath environments using the standard IEEE 802.15.3a channel models. The proposed subsampling receiver provides an attractive digital alternative to the classical approach based on analog correlations, and can reach data rates above 100 Mb/s.**

I. Introduction

Ultra-wideband (UWB) has the potential of delivering very high data rates over short distances for Wireless Personal Area Networks (WPAN) communications. Current proposals for standardisation target a maximum data rate of 480 Mbps at a distance of 2 meters. Ultra Wideband signals for communication applications, as specified by the FCC [1], have a minimum bandwidth of 500 MHz and operate within the 3.1 to 10.6 GHz frequency band. This paper focuses on pulsed UWB systems which transmit information as a sequence of very short pulses utilizing the whole available bandwidth.

Designing UWB receivers presents unique challenges. The optimum receiver is based on matched filtering (correlation) with the transmitted pulse followed by a RAKE structure capturing the multipath diversity of the channel. However the transmitted pulse is distorted by the transceiver antennas and the channel [2]. As this pulse distortion can vary among the multipaths, the RAKE receiver can not achieve the optimal performance. Moreover, the high number of resolvable paths present in typical UWB channels requires a RAKE with a high number of fingers. Transmitted reference (TR) systems [3], [4] avoid the need for local template generation by transmitting modulated and unmodulated versions of the pulse. This technique simplifies the receiver structure but requires carefully implemented delay lines in the analog domain. On the other hand, digital based receivers provide more flexibility and benefit from CMOS technology scaling, but require ADCs sampling at Nyquist rate which are hardly realizable and highly power consuming. Parallel ADC architectures based on signal channelization in time [5], [6] or frequency domain [7] reach an aggregate sampling rate equivalent to Nyquist's criterion at the cost of increased area, and require careful design of the PLL controlling the sampling time and appropriate techniques to compensate circuit mismatches between the parallel branches. Subsampling techniques alleviate this issue. For example, a direct sampling approach is used in [8]. However, it is only applicable for signals in the 3–5 GHz band and still requires a 2 GSamples/s ADC.

This paper assesses the performance of a flexible subsampling receiver based on line spectrum estimation techniques applied in the frequency domain in order to recover the position and the amplitude of the pulses. Such receiver provides the flexibility of a digital implementation without the high power consumption or area penalty caused by a fast running or several low-speed ADC's. Moreover, multicode spread spectrum techniques are applied to provide bandwidth on demand to the user by dynamically adapting the length and number of codes used. As a result, the proposed receiver provides a power efficient and flexible alternative to traditional UWB receivers.

II. Application of Subsampling Techniques to Pulsed UWB Signals

A. Signal Model and Subsampled Pulse Detection Algorithms

As shown in [9], particular classes of signals with infinite bandwidth, such as repetitive streams of Diracs, can be sampled. These signals must first be low-pass or bandpass filtered before they are sampled at a multiple of their *rate of innovation* $\rho = 2K/T_f$, where T_f is the period of the stream and K the number of Diracs per period. Parametric PSD estimation methods can then be applied in the frequency domain to estimate the position of the Diracs.

As an application of this result, a received pulsed UWB signal $s_{rx}(t)$ can be modelled as the convolution between a stream of Diracs sent at the frame rate T_f, the received pulse shape $p_{rx}(t)$, and the channel $h(t)$:

$$s_{rx}(t) = p_{rx}(t) \otimes h(t) \otimes \sum_{n=-\infty}^{+\infty} \sum_{k=1}^{K} c_{n,k}\delta(t - nT_f - t_{n,k}) + n(t) \tag{1}$$

where $c_{n,k} \in \{0, \pm\Gamma, \pm 3\Gamma, \dots\}$ and $t_{n,k} \in \{0, \Delta, 2\Delta, \dots\}$ are the data streams modulating the K pulse amplitudes and positions, respectively, and $n(t)$ is the received noise. This model is valid provided that the channel $h(t)$ does not modify the pulse shape, i.e. $h(t) = \sum_{i=1}^{N_p} \alpha_i \delta(t - \tau_i)$, where N_p is the total number of paths. Line spectrum PSD estimation

methods can be used to retrieve the position of the pulses after deconvolving the received signal by the pulse shape, as suggested by [10]. In this case, N_p pulses must be estimated using line spectrum methods of order N_p, which is very high for typical UWB channels. In the case of the IEEE 802.15.3a standard channel models CM1–CM4 [11], for example, the number of paths capturing 85% of the channel energy ranges between 25 and 175. A reduced set of principal components is therefore estimated in [10]. The deconvolution is done by dividing in the frequency domain the sampled received signal $FFT(s_{rx}[n])$ by the pulse spectrum $FFT(p_{rx}[n])$. However, a high order is still required (>10 for CM1) and affects the receiver complexity and the sampling rate, which are proportional to the order. Moreover, it is assumed that the received pulse shape is known at the receiver, while it can differ significantly from the transmitted pulse shape. Pulse distortion is caused in particular by the transceiver antennas if these do not have a constant gain and linear phase frequency response. Such distortion is hard to estimate independently from the channel effect. The model (1) is not applicable when the frequency selective distortion caused by the channel and the impact of the antennas are taken into account, leading instead to a more realistic model of the form

$$s_{rx}(t) = h_c(t) \otimes \sum_{n=-\infty}^{+\infty} \sum_{k=1}^{K} c_{n,k}\delta(t - nT_f - t_{n,k}) + n(t) \quad (2)$$

where $h_c(t) = \sum_{i=1}^{N_p} \alpha_i p_i(t - \tau_i)$ is the compound channel impulse response, which includes the distortion caused by the antennas and the dispersive behavior of the building materials in the propagation channel. The deconvolution by the pulse shape can therefore not be applied. A polynomial model for the frequency domain representation of $h_c(t)$ is proposed in [12]. However, this approach again increases the sampling rate by the polynomial order. Instead, this paper assesses the performance of the deconvolution of the received signal by the compound channel, followed by a line spectrum PSD estimation method of minimal order. This approach was suggested in [13] but focused on binary PAM in AWGN conditions only.

B. Basic Principles of the Line Spectrum Receiver

The received signal $s_{rx}(t)$ is filtered and sampled following [9] and $2M + 1$ frequency domain samples $\mathbf{y} = [y[-M], \ldots, y[M]]$ are available, with $M \geq K$. Let $\mathbf{H}_{fc}$ be defined as a diagonal matrix with the $2M+1$ frequency domain representation of the filtered compound channel. For the sake of simplicity, we consider here a single user system and do not take the PN spreading into account. The received signal in the frequency domain $\mathbf{y}$ can be expressed as

$$\mathbf{y} = T_f^{-1}\mathbf{H}_{fc}\mathbf{A}\mathbf{c} + \mathbf{n} \quad (3)$$

where $\mathbf{n}$ corresponds to the filtered noise in the frequency domain, $\mathbf{A} = [\mathbf{a}_1 \ \ldots \ \mathbf{a}_K]$, $\mathbf{a_k} = \left[z_k^{-M}, \ldots, z_k^{M}\right]$ with $z_k = e^{-2\pi j t_k/T_f}$, and $\mathbf{c} = [c_1, \ldots, c_K]$. We omit n in $t_{n,k}$ and $c_{n,k}$ since we focus on a single frame. The filtered compound channel impulse response $h_{fc}(t)$ is assumed available via appropriate training of the receiver using a known preamble sent at the beginning of the data stream. The deconvolution by $h_{fc}(t)$ can be simply implemented as a division in the frequency domain $\mathbf{y}_{eq} = \mathbf{H}_{fc}^{-1}\mathbf{y}$ at the cost of possible noise enhancement caused by amplitude dips of the channel frequency response. A conventional line spectrum method of order K such as ESPRIT is then applied to the equalized signal $\mathbf{y}_{eq}$ to estimate the positions $\left\{\hat{t}_i\right\}_{i=1}^{K}$. The estimated amplitudes $\{\hat{c}_i\}_{i=1}^{K}$ are the solution of the system (3) which can be solved by least-squares (LS) or total LS techniques.

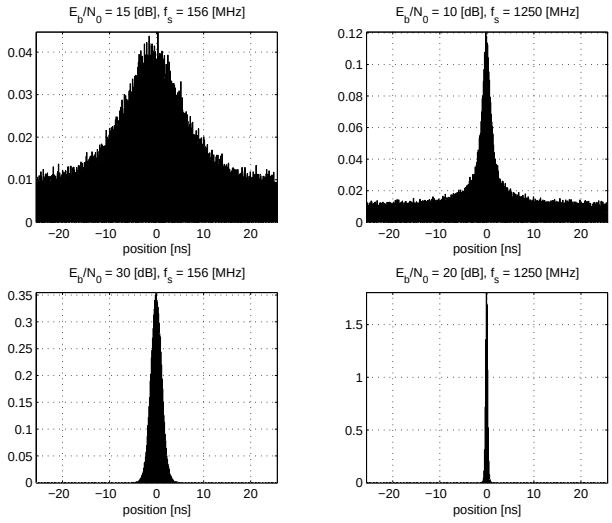

Fig. 1. Examples of PDF of the Estimated Pulse Position.

III. Performance of the Subsampling Receiver

The line spectrum subsampling receiver has been simulated with an AWGN channel as well as using the IEEE 802.15.3a standard channel models [11]. The adopted SNR definition is as follows. Given a desired $(E_b/N_0)_{des}$, the AWGN noise power added to the receiver input signal is

$$\sigma_n^2 = \frac{\sigma_s^2}{(E_b/N_0)_{des}} \cdot \frac{W}{1/T_f} \quad (4)$$

where σ_s^2 is the average signal power and W the model bandwidth. This definition allows for a fair comparison of the receiver performance when using different pulse types and filter bandwidths. Although the simulation results presented in this paper have been obtained with the second derivative of the gaussian monocycle, no significant difference was observed with other pulses.

Different receiver bandwidths and sampling rates have been simulated, and a single pulse per period is assumed ($K = 1$). The pulse repetition period is high enough ($T_f = 51.2$ ns) to avoid inter pulse interference (IPI). The central frequency f_c of the receiver bandpass filter is chosen as the maximum of the pulse PSD.

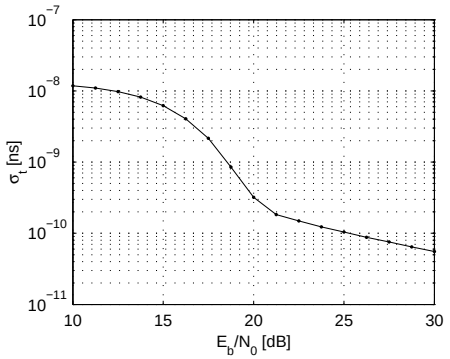

Fig. 2. RMSE Estimated Position, $f_s = 1.25$ GHz.

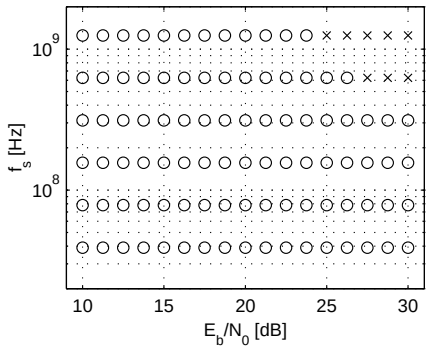

Fig. 3. Normality Test of the Estimated Pulse Position: H_0 Rejection (o) and No Rejection (x).

A. Distribution of the Estimated Position and BER for PPM

Figure 1 shows typical examples of the distribution of the position estimated by ESPRIT for different levels of E_b/N_0 and sampling rates in an AWGN channel. At low E_b/N_0 and sampling rate, the error on the estimated pulse position can be in the order of magnitude of the pulse repetition period. This extreme situation is not suitable for reliable communication. At higher E_b/N_0 or sampling rates, the root mean squared error (RMSE) of the estimated pulse position σ_t decreases linearly with E_b/N_0 (fig. 2), and the pulse position can be very accurately estimated with a maximum error below 1 ns at $E_b/N_0 > 20$ dB. A remarkable advantage [14] of line spectrum methods in this context is the dependency in $\mathcal{O}(N^{-3/2})$ of σ_t with the number of available samples ($N = 2M+1$), i.e. with the receiver bandwidth and the ADC sampling rate. As a result, the performance improves rapidly with increasing bandwidths.

The probability density function (PDF) of the estimated position depends on E_b/N_0 and the number of samples. At low E_b/N_0 and sampling rates, it presents a heavy tail which causes the rejection of the null hypothesis of a normal distribution at 5% confidence level by a Kolmogorov-Smirnov (K-S) test. Indeed, it is known that the estimates of sinusoidal frequencies using subspace rotation techniques are not gaussian distributed [14], although the distribution is asymptotically normal [15]. The number of available samples from subsampled UWB signals, with a pulse repetition rate and a sampling rate in the order of magnitude of tens to hundreds of MHz, is typically too small compared to the asymptotic case although the K-S test becomes positive at higher E_b/N_0 and sampling rates (fig. 3). In the typical UWB conditions, the PDF of the estimated pulse position is closer to a Laplace distribution with a uniform error floor which depends on E_b/N_0 and the sampling rate.

Figure 4 shows typical BER curves for binary PPM as a function of the modulation index Δ for several sampling rates. As the bandwidth and sampling rates double, the optimal BER curves for PPM improve by approximately 2.5 dB. Higher sampling rates allow resorting to smaller modulation indices. The accuracy of the position estimation which can be achieved enables high order PPM and data rates, as Δ can be chosen

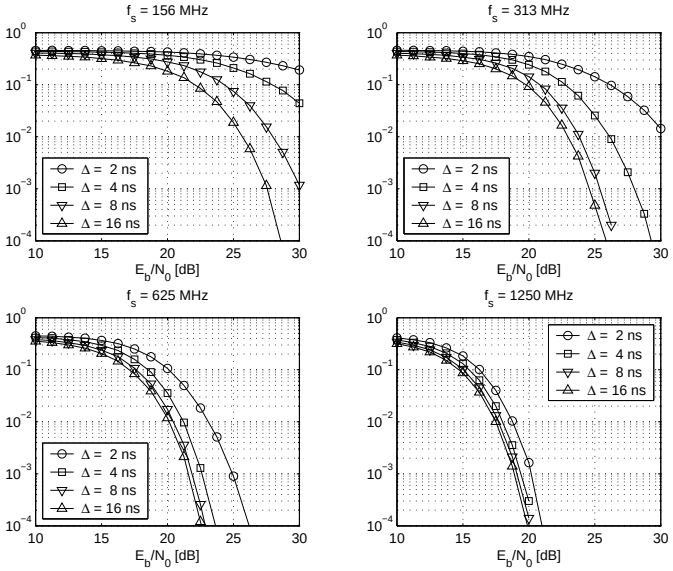

Fig. 4. BER for 2-PPM, AWGN Channel.

slighly above the pulse duration. As an example, a 16-PPM is feasible at $f_s = 32/T_f = 625$ MHz with $T_f = 51.2$ ns.

The performance is significantly worse in multipath conditions, however, due to the noise enhancement caused by the zero-forcing equalizer. Fig. 5 shows the binary PPM BER curves averaged over 100 realizations of the IEEE 802.15.3a channel model 1 (CM1) for the same sampling rates as fig. 4. The error floor on the PDF decreases more slowly with the sampling rate and E_b/N_0 than previously, which causes a higher RMSE σ_t. The resulting heavy tail causes the K-S test to reject the hypothesis of a normal distribution even at high sampling rates. The performance strongly depends on the particular realization of the channel model. As an example, figure 6 corresponds to the first realization of CM1. Contrary to the AWGN case, the performance does not necessarily improve with higher bandwidths and sampling rates. A larger bandwidth may capture dips of the channel frequency response which annihilate the gain of having more available samples. In this example, a low order PPM (with a large modulation index) can be best realized with a sampling rate of $8/T_f = 156$ MHz.

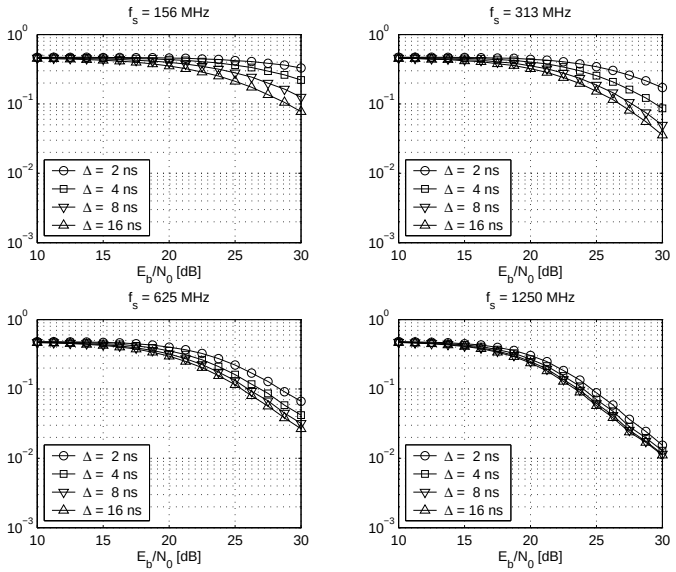

Fig. 5. BER for PPM, Average IEEE 802.15.3.a Channel CM1.

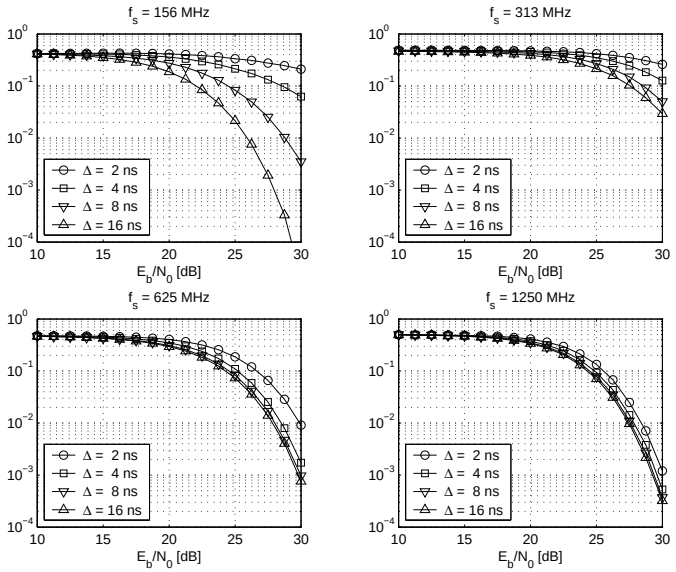

Fig. 6. BER for PPM, IEEE 802.15.3.a Channel CM1, Realization nr. 1.

Similar conclusions apply to the other IEEE channel models CM2–CM4. The choice of the optimal central frequency, RF filter bandwidth and ADC sampling rate can be performed during the training of the receiver but requires a configurable front-end. Section V provides more details about flexible architectures satisfying this requirement.

B. Distribution of the Estimated Amplitude and BER for PAM

The estimated amplitude follows a normal distribution at high sampling rate, like for PPM. Figure 7 (left) illustrates the BER performance of binary PAM and confirms preliminary results for an AWGN channel [13]. These BER curves are similar to the optimum PPM (fig. 4). As a consequence, the data can be sent using PPM and PAM in parallel without

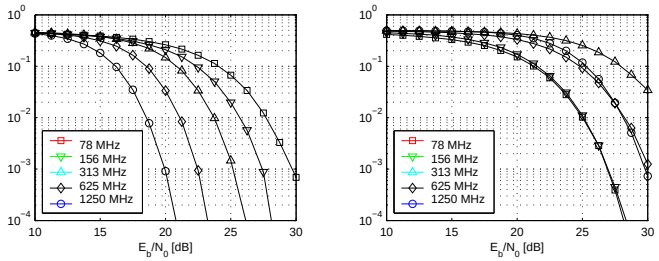

Fig. 7. BER for binary PAM, AWGN Channel (left) and CM1 nr. 1 (right).

different error coding techniques. A more optimal coding technique would take into account the correlation between the errors on the bits carried via PPM and PAM due to eq. (3).

Like for PPM, the BER performance for PAM is affected by multipath conditions (fig. 7, right) but can be optimized by appropriately selecting the central frequency and bandwidth of the RF filter.

IV. Link Budget

We follow in this paper the guidelines of the IEEE 802.15.3a Task Group [16] for UWB link budgets, based on classical narrowband link budgets using Friis transmission formula $P_r = \left(P_t G_t \lambda^2\right) / \left(4\pi d\right)^2$ with geometric average frequency $f_c' = \sqrt{f_{min} f_{max}}$. The technical justification for using narrowband path loss calculations relies on perfect isotropically radiating antennas at the transmitter and receiver.

The first case in table I illustrates the link budget for PAM and PPM, assuming a sampling rate equal to $32/T_f = 625$ MHz, a target data rate of 110 Mb/s and a channel coding gain of one order of magnitude. The minimum Rx sensitivity level is defined as the minimum required average Rx power for a received symbol in AWGN. The link budget is negative at the target data rate because it filters out an important fraction $1-F$ of the signal bandwidth and only captures a limited amount of energy FE_b. As a consequence, the rate at which the receiver accumulates the signal energy is reduced by a factor F. On the other hand, narrowband interference can easily be rejected by avoiding the affected subband (i.e. interference excision).

The link budget can be made positive by channelizing the data using N_c orthogonal (Walsh) codes of length $L_c \geq N_c$. The transmitter converts the data stream into N_c lower rate streams which are each encoded with a different code. As an example, the second case in table I assumes $L_c = N_c = 16$.

Constructive addition between the streams and high peak-to-RMS ratios can be avoided by sending the pulses of each basic stream with a different time offset which is a multiple of T_f/N_c. Avoiding constructive pulses is desirable as these increase the risk of violating the FCC peak emission limits [1] and complicate the design of the receiver's analog part.

At a fixed pulse repetition rate, using more and longer Walsh codes improves the link budget (case 3 in table I) but does not augment the total data rate. Longer codes increase the number of parallel streams which can be sent *and* the number of pulses per bit. The net data rate is therefore the same but

TABLE I

LINK BUDGET FOR LINE SPECTRUM SUBSAMPLING RECEIVER

Term	*case 1*	*case 2*	*case 3*	*Unit*	*Comment*
$R_{b,tot}$	110	110	110	Mb/s	Bit rate
L_c	—	16	32	—	Walsh code length
R_b	110	6.875	3.348	Mb/s	Bit rate for each channel
P_t	-2.5	-2.5	-2.5	dBm	Average Tx power, assuming -41.3 dBm/MHz between $f_{min} = 3.1$ and $f_{max} = 10.6$ GHz
G_t	0	0	0	dBi	Tx antenna gain (isotropic antenna)
$f_c^{'}$	5.7	5.7	5.7	GHz	Geometric central frequency ($f_c^{'} = \sqrt{f_{min} f_{max}}$)
PL_{1m}	47.6	47.6	47.6	dB	Path loss at 1 m and at $f_c^{'}$ ($PL_{1m} = 20\log_{10}(4\pi f'_c/c)$)
PL_{10m}	20	20	20	dB	Extra path loss at $d = 10$ m ($PL_{10m} = 20\log_{10}(d)$)
G_r	0	0	0	dB	Rx antenna gain (isotropic antenna)
P_r	-70.2	-70.2	-70.2	dBm	Rx power ($P_t + G_t - PL_{1m} - PL_{10m} + G_r$)
N_0	-174	-174	-174	dBm/Hz	Noise PSD (kT, with $T = 290$ K)
N_b	-93.6	-105.6	-108.6	dBm	Average noise power per bit ($N_0 + 10\log_{10}(R_b)$)
NF	7	7	7	dB	Rx noise figure referred to the antenna terminal [11]
P_n	-86.6	-98.6	-101.6	dBm/s	Total average noise power per bit ($P_n = N_b + NF$)
$(E_b/N_0)_{min}$	23	23	23	—	Minimum E_b/N_0 to reach BER=$1e^{-5}$ (AWGN channel)
I	2.5	2.5	2.5	dB	Implementation loss [11]
M	**-9.1**	**3**	**6**	—	Link margin ($M = P_r - P_n - (E_b/N_0)_{min} - I$)
T_f	50	50	50	ns	Pulse Period
B	16	16	16	—	Receiver bandwidth (in multiples of $1/T_f$)
f_s	320	320	320	MHz	Sampling rate ($f_s = B/T_f$)
R_{symb}	20	1.25	0.625	Msymb/s	Symbol rate ($R_{symb} = 1/(L_c T_f)$)
b	5.5	5.5	5.5	bits/symb	Bits per symbol ($b = R_b/R_{symb}$)

the coding gain has improved. The number of bits per symbol is independent of the Walsh code length, since

$$b = \frac{R_b}{R_{symb}} = \frac{R_{b,tot}/N_c}{1/(L_c T_f)} = \frac{R_{b,tot}/L_c}{1/(L_c T_f)} = R_{b,tot} T_f \qquad (5)$$

Consequently, the two options to increase $R_{b,tot}$ and reach higher data rates are 1) to reduce the pulse period T_f, until the IPI affects the BER performance, 2) to maximize b by resorting to high order PPM and/or PAM. However, the receiver complexity increases with the length and the number of codes, in particular the memory requirements. N_c parallel streams must be accumulated before being processed by the FFT and the algorithm estimating the pulse position and amplitude. Moreover, the power consumption of the transmitter is proportional to the number of codes, since each stream is sent at the maximum power tolerated by the FCC. The receiver's power consumption is related to the computation cost and affects the dynamic and static (leakage) power consumption.

Channelized streams allow matching dynamically the data rate and quality of service (QoS) according to the user's needs. For a fixed length L_c and a given E_b/N_0, less streams $N_c < L_c$ may be sent if the user's application has temporarily lower requirements in terms of data rate. As a consequence, the power consumption of the transmitter is reduced by a factor N_c/L_c with respect to the peak transmission power. At the receiver side, less computation power is required to process $N_c < L_c$ streams, which also translates into lower power consumption if appropriate shutdown mechanisms are implemented. When the application requires higher transmission rates, the transmitter sends the data using all possible channels and reaches the peak transmission rate. The information concerning the actual number of codes used by the transmitter can be preliminary sent in a header within the preamble of each transmitted packet.

V. RECEIVER ARCHITECTURE

A possible receiver architecture is shown in figure 8. A fraction of the total signal bandwidth is selected by configurable filters and mixer in the analog front-end. The sampling rate depends on the filter's bandwidths and can range from a few multiples of the pulse repetition rate up to hundreds of MHz.

A direct bandpass sampling architecture [8] should be avoided in the present case, as it suffers from severe requirements on aperture jitter and noise folding. Assuming a worst case analysis based on the classical aperture jitter noise model $SNR_{aj} = -20\log(2\pi f_{max}\sigma_{Taj})$, where $f_{max} = 10.6$ GHz, the RMS value of the aperture jitter σ_{Taj} should be in the order of magnitude of picoseconds for the aperture noise to be negligible with respect to the available SNR. In addition, the wideband noise at the sampling circuitry is aliased to the signal band. This noise folding issue is exacerbated by the extreme subsampling factor f_c/f_s.

A direct conversion architecture is therefore preferable. However, DC offset and IQ imbalance must be compensated in the digital part.The transmitter sends several low rate data streams in parallel using orthogonal spreading codes on top op classical direct sequence spreading. The streams are despread at the receiver after the non-idealities of the analog front-end are compensated. A preliminary analysis indicated that the ADC bit width requirements are moderate (3–4 bits), which guarantees a low power consumption. After channel equalization, line spectrum estimation techniques are applied to each stream in the frequency domain in order to recover the position of the pulses, followed by the amplitude estimation.

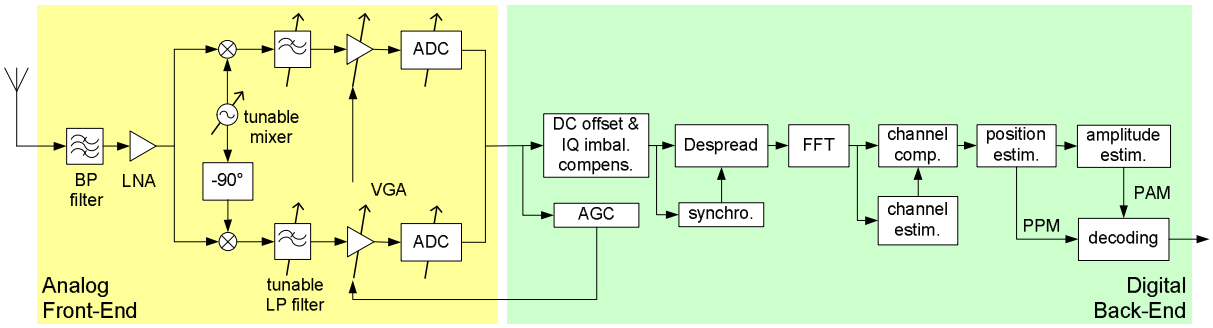

Fig. 8. Subsampling Receiver Architecture, Band Selection in the Analog Domain.

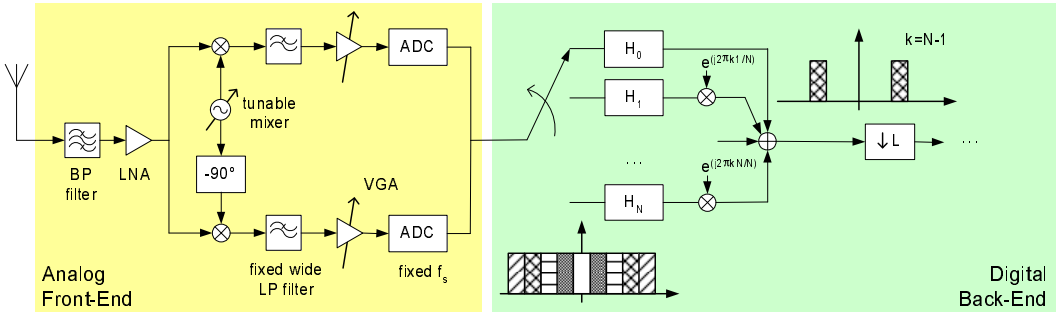

Fig. 9. Subsampling Receiver Architecture, Band Selection in the Digital Domain.

The digital back-end after the despreading block is working at symbol rate. The intensive and repetitive signal processing functions in the digital back-end provide several opportunities for design space exploration.

An alternative architecture is shown in figure 9, where the sampling rate and filter's bandwidths are fixed at a high value (e.g. about 500 MHz). The mixer frequency is tunable and the optimal subband within the spectrum window of the RF filters is selected in the digital domain. Although this structure continuously works at the maximum sampling rate which is tolerated by implementation concerns and power consumption requirements, it allows a more flexible selection of the optimal central frequency and bandwidth.

VI. Conclusion

This paper has presented and assessed a flexible and digital based subsampling receiver in the 3.1–10.6 GHz frequency band. Channelization techniques are used to accommodate for time-varying rate and QoS requirements of the user. High data rates can be achieved despite very low sampling rates. The proposed receiver enables the development of cross-layer optimization algorithms which adapt the transmission characteristics at the physical layer to the application requirements. Future work will concentrate on practical implementation of this receiver.

References

[1] FCC, "First Report and Order, Revision of Part 15 of the Commissions Rules Regarding Ultra-Wideband Transmission Systems," April 2002.

[2] R. Scholtz, D. Pozar, and W. Namgoong, "Ultra-Wideband Radio," *EURASIP J. Applied Signal Proc.*, vol. 3, pp. 252–272, 2005.

[3] R. Hoctor and H. Tomlinson, "Delay-Hopped Transmitted-Reference RF Communications," in *Proc. IEEE Conference on Ultra Wideband Systems and Technologies*, May 2002, pp. 265–270.

[4] G. Leus and A.-J. van der Veen, "A Weighted Autocorrelation Receiver for Transmitted Reference UWB Systems," in *Proc. IEEE Workshop on Signal Proc. Advances in Wireless Comm. (SPAWC)*, June 2005.

[5] I. O'Donnell, M. Chen, S. Wang, and R. Brodersen, "An Integrated, Low Power, Ultra-Wideband Transceiver Architecture," in *IEEE CAS Workshop on Wireless Communications and Networking*, Sept. 2002.

[6] B. Blazquez, P. Newaskar, F. Lee, and A. Chandrakasan, "A Baseband Processor for Pulsed Ultra-Wideband Signals," in *IEEE Custom Integrated Circuits Conference*, Oct. 2004.

[7] N. W. Feng, L., "An Oversampled Channelized UWB Receiver," in *IEEE Ultra Wideband Systems and Technologies (UWBST)*, May 2004.

[8] M. Chen and R. Brodersen, "A Subsampling UWB Impulse Radio Architecture Utilizing Analytic Signaling," *IEICE Trans. Electronics*, vol. E88-C, no. 6, pp. 1114–1121, 2005.

[9] M. Vetterli, P. Marziliano, and T. Blu, "Sampling signals with finite rate of innovation," *IEEE Trans. Signal Proc.*, vol. 50, pp. 1417–1428, 2002.

[10] J. Zhang, T. Abhayapala, and R. Kennedy, "Principal Components Tracking Algorithms for Synchronization and Channel Identification in UWB Systems," in *IEEE Eighth Int. Symposium on Spread Spectrum Techniques and Applications*, Sept. 2004, pp. 369–373.

[11] J. Foerster, "Channel Modeling Sub-Committee Report Final (IEEE P802.15-02/490r1-SG3a)," 2003.

[12] I. Maravić and M. Vetterli, "Low-Complexity Subspace Methods for Channel Estimation and Synchronization in Ultra-Wideband Systems," in *Proc. International Workshop on UWB Systems*, June 2003.

[13] J. Kusuma, A. Ridolfi, and M. Vetterli, "Sampling of Communication Systems with Bandwidth Expansion," in *Proc. ICC*, May 2002.

[14] P. Stoica and T. Söderström, "Statistical Analysis of MUSIC and Subspace Rotation Estimates of Sinusoidal Frequencies," *IEEE Trans. Signal Proc.*, vol. 39, pp. 1836–1847, 1991.

[15] J.-P. Delmas, "Asymptotic Performance of Second-Order Algorithms," *IEEE Trans. Signal Proc.*, vol. 50, pp. 49–57, 2002.

[16] K. Siwiak, J. Ellis, and R. Roberts, "802.15.3TGa Alternate PHY Selection Criteria (IEEE P802.15-03/031r5)," 2002.